WIND ENERGY
Wind Energ. 2018; **00**:1–**??**
DOI: 10.1002/we

RESEARCH ARTICLE

Passive vibration control of an offshore floating hydrostatic wind turbine model

Xin Tong[1], Xiaowei Zhao[1], and Aris Karcanias[2]

[1]School of Engineering, University of Warwick, Coventry, CV4 7AL, United Kingdom.
[2]FTI Consulting, 200 Aldersgate, Aldersgate Street, London, EC1A 4HD, United Kingdom.

ABSTRACT

We propose to make use of the hydraulic reservoir of a floating barge hydrostatic wind turbine (HWT) to suppress the pitch and roll motions of the barge by making the reservoir into a shape of an annular rectangular to serve as a bidirectional tuned liquid column damper (BTLCD). This means we have made a barge-motion damper with negligible extra costs as an HWT needs a reservoir for fluid storage anyway. The barge HWT simulation model is transformed from the NREL (National Renewable Energy Laboratory) 5-MW geared equipped ITI Energy barge wind turbine model within the FAST (Fatigue, Aerodynamics, Structures, and Turbulence) code by replacing its drivetrain with a hydrostatic transmission drivetrain and incorporating the coupled dynamics of the barge-reservoir system. We use two simplified turbine-reservoir models to optimise the parameters of the BTLCD reservoir, which describe the pitch and roll motions of the turbine-reservoir system respectively. Simulation results based on the transformed NREL 5-MW barge HWT model show that the optimal BTLCD reservoir is very effective in mitigating pitch and roll motions of the barge under realistic wind and wave excitations, which reduces the tower load and improves the power quality.

KEYWORDS

offshore hydrostatic wind turbine; floating platform; vibration control; bidirectional tuned liquid column damper; optimisation

Correspondence
Xiaowei Zhao, School of Engineering, University of Warwick, Coventry, CV4 7AL, United Kingdom.
E-mail: xiaowei.zhao@warwick.ac.uk.
Tel.: +44 (0)24 765 23145.
Fax: +44 (0)24 76 418922.

Received . . .

1. INTRODUCTION

Wind power has been used as a clean source of renewable energy with sustainable growth in penetration and investments. To harvest more frequent and stronger winds, large wind turbines are being increasingly installed offshore. However, a large offshore wind turbine has a massive and heavy nacelle (including components inside it) with a strong supporting tower, whose transportation and installation are very difficult and expensive [1, 2]. In addition, the gearbox of the conventional wind turbine drivetrain is very expensive and fragile [3], whose replacement is difficult and costly in particularly for the offshore application [1]. Electromechanical coupling of vibrations including impact on drivetrain and generators could be significant and studies on such effects have been reported [4, 5]. Replacing the gearbox drivetrain with a hydrostatic transmission (HST) drivetrain is a good way to solve these problems. The latter has a much longer life cycle than the gearbox drivetrain and can also reduce the tower-top mass. A wind turbine with an HST drivetrain is called a hydrostatic wind turbine (HWT). Figure 1 (taken from Dutta [6]) represents a typical HST drivetrain. The rotor is directly coupled to a hydraulic pump in the nacelle, which forces the hydraulic oil into the closed oil circuit. The high pressurised oil drives a hydraulic motor, which is coupled with a generator to produce electric power to the grid. The low pressure line transports the low pressure oil back to the pump from the motor. In terms of power conversion, the pump first converts the rotor/pump shaft power to hydraulic power, which is then converted to the motor/generator shaft power through the motor [1]. Finally, the motor/generator shaft power is converted to electric power through the generator. An HST generally needs a hydraulic reservoir as an auxiliary device. A portion of the hydraulic fluid outputted by the motor should be imported to the reservoir

Prepared using weauth.cls [Version: 2010/06/17 v1.00]

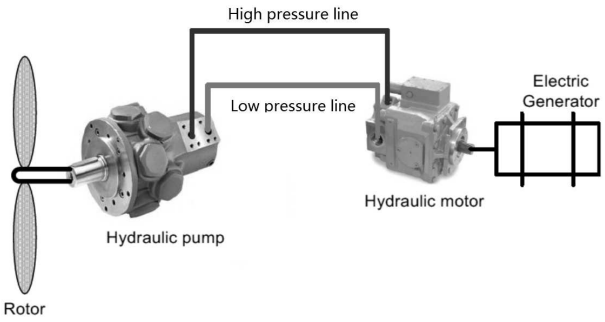

Figure 1. Main components of a typical HST drivetrain in the HWT, as well as their connections. This figure is taken from the thesis by Dutta [6].

for heat dissipation, contaminant settling and deaeration [1, 7]. Meanwhile, equivalent amount of fluid should be charged into the low pressure line from the reservoir for circulation.

Vibration suppression in wind turbines and floating offshore wind turbines specifically is a topical area of research, and use of passive, active and semi-active controllers have been investigated [8, 9, 10, 11, 12, 13]. In this paper, we conduct research on an offshore hydrostatic wind turbine (HWT) with a floating barge platform. The barge rotational motions not only cause large fluctuations in the rotor speed and generator power, but also cause considerable load variations on the turbine, especially on the tower base [14]. Hence, it is of critical significance to develop control techniques to suppress these motions to improve energy capture, increase the tower's life expectancy and enable the construction of lighter and cheaper wind turbine towers. As a spin-off application, we propose to make use of the reservoir as a bidirectional tuned liquid column damper (BTLCD) to damp pitch and roll responses of the barge. The BTLCD reservoir can be placed on the floating barge of the HWT.

A tuned liquid column damper (TLCD) is a U-shaped tube partially filled with liquid. Its vibration frequency is required to be tuned to a dominant modal frequency of the primary structure to suppress the structural motions through the gravitational restoring force acting on the displaced liquid. Energy is dissipated through one or more orifices within the horizontal column of the TLCD [15]. Orifice damping has an important effect on suppression of vibrations [16]. The TLCD has been demonstrated to be effective in mitigating structural vibrations induced by winds, earthquakes and waves [17, 18, 19, 20]. Explicit expressions of the optimal TLCD parameters were given in the literature [21, 22], which are only feasible for undamped primary structures with one degree of freedom (DOF) subject to white noise excitations. Under other circumstances, optimal TLCDs were designed to suppress structural translational motions through numerical optimisation approaches [23, 22]. For structures in rotational motions, Xue et al. [24] validated that the TLCD could effectively damp structural pitch motions. Wu et al. [25] modelled the interaction between the TLCD and the primary structure in pitch motions more accurately, by employing the Lagrange's equation approach.

In terms of the application of the TLCD in wind turbines, Colwell and Basu [26] placed a TLCD on top of a monopile wind turbine tower to demonstrate its feasibility for tower pitch suppression. Roderick [27] investigated to employ the TLCD to reduce tower pitch vibrations of offshore wind turbines with three types of platforms, i.e., the fixed-bottom monopile, the floating barge and the floating spar buoy. They optimised the TLCD parameters through a deterministic sweep, which searched among a number of feasible combinations of parameter values to minimise the standard deviation of tower-top displacements. Their optimisation and simulation tests were both based on simplified models consisting of TLCD dynamics, the first tower fore-aft bending DOF, and the platform pitch displacement DOF (only for the cases of floating barge and spar buoy wind turbines). Coudurier et al. [28] designed a TLCD to damp pitch motions of the MIT/NREL 5-MW barge wind turbine. They optimised TLCD parameters through minimising the peak pitch response to harmonic wave excitations in a frequency range which was likely to excite the turbine pitch mode, by using Matlab optimisation function *fmincon*. Their optimisation was based on a simplified model containing TLCD dynamics and the barge pitch DOF while the simulation was based on a low fidelity barge wind turbine model including TLCD dynamics and the DOFs of barge surge, heave and pitch, which showed that the optimal TLCD performed well. Basu et al. [29] proposed a new type of TLCD for suppressing edgewise vibrations of offshore turbine blades.

Because the TLCD can only damp vibrations in one direction, bidirectional liquid dampers have been introduced in order to suppress the structural vibrations in two perpendicular directions. Hitchcock et al. [30] designed a BTLCD comprising multiple TLCDs sharing a common horizontal liquid mass. Lee et al. [31] introduced a tuned liquid column and sloshing damper (TLCSD), which works as a TLCD and a tuned liquid sloshing damper (TLSD) in two perpendicular directions, respectively. However, it is very difficult to tune TLSD parameters because the frequency and damping ratio of the TLSD increase non-linearly with the amplitude of the excitation. Rozas et al. [32] proposed a type of BTLCD which not only

Wind Energ. 2018; **00**:1–?? © 2018 John Wiley & Sons, Ltd.
DOI: 10.1002/we
Prepared using weauth.cls

required less liquid but also had a simpler mathematical model which makes the parameter optimisation easier compared with the TLCSD. In the present paper, we adapt this type of BTLCD configuration for the reservoir to damp pitch and roll motions of the HWT barge in the fore-aft and side-to-side directions. We mention that the BTLCD devised by Rozas et al. [32] was used to reduce vibrations in two perpendicular translational directions.

In order to conduct detailed simulation test, we transform the well-known NREL (National Renewable Energy Laboratory) 5-MW baseline (geared equipped) ITI Energy barge wind turbine model within FAST (Fatigue, Aerodynamics, Structures, and Turbulence) into a detailed aero-hydro-servo-elastic barge HWT model with a BTLCD reservoir placed on the barge. But our optimal BTLCD design is based on two simplified mathematical models which describe the fore-aft (pitch) and side-to-side (roll) motions of the turbine-reservoir system, respectively. Since the fore-aft direction bears the largest loading from winds and waves, we first optimise the BTLCD reservoir parameters based on the model relevant to this direction. Then we optimise the remaining parameters based on the other model. We derive optimal parameters for the BTLCD reservoir through multistart optimisation, i.e., running the MATLAB optimisation solver *fmincon* from multiple randomly selected starting points to obtain a local minimum. FAST simulation results show that our optimal BTLCD reservoir achieves very good performances in mitigating barge pitch and roll motions of the transformed NREL 5-MW HWT model, which reduces the tower-base damage load and improves the power quality.

The structure of the paper is as follows. In Section 3, we transform the NREL 5-MW baseline (geared equipped) ITI Energy barge wind turbine model within FAST to an HWT with a BTLCD reservoir mounted on top of its barge. Here we focus on incorporating the coupled dynamics of the barge-reservoir system into the FAST code. In Section 4, we optimise the parameters of the BTLCD reservoir, based on two simplified mathematical models respectively describing the fore-aft (pitch) and side-to-side (roll) motions of the turbine-reservoir system. In Section 5, we test the performance of the optimal BTLCD reservoir in suppressing the barge pitch and roll motions based on the transformed NREL 5-MW barge HWT model. Finally in Section 6 we conclude this paper.

2. NREL 5-MW BASELINE BARGE WIND TURBINE MODEL AND NREL COMPUTER-AIDED ENGINEERING TOOLS

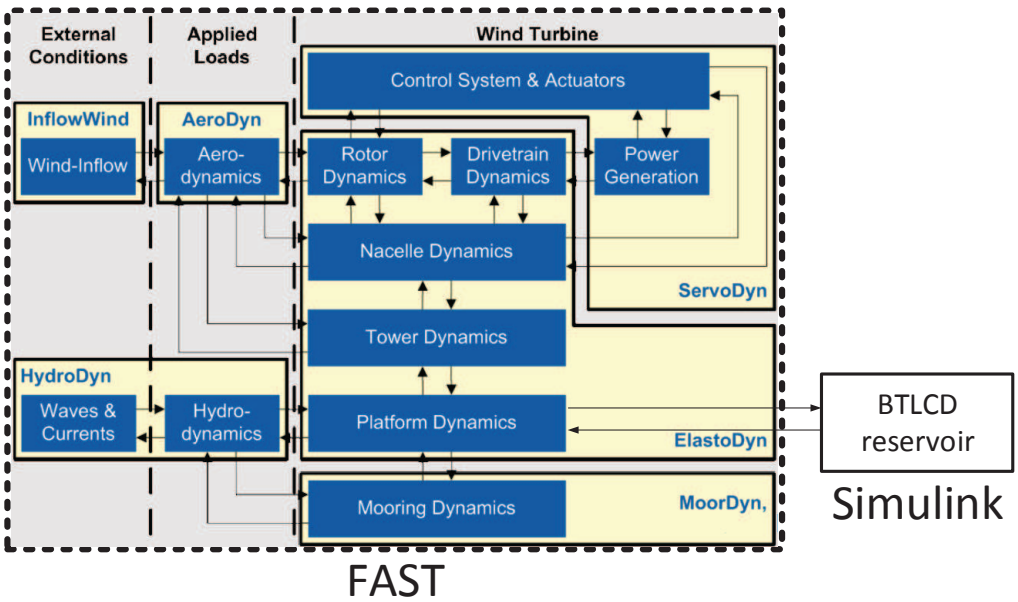

Figure 2. Schematic of FAST modules (in the dashed block) [33] coupled with a BTLCD reservoir modelled in MATLAB/Simulink for the barge HWT.

The NREL 5-MW baseline ITI Energy barge wind turbine model [14] represents a type of typical geared equipped variable-speed variable-pitch floating offshore wind turbine. It has a 6-DOF (surge, sway, heave, roll, pitch and yaw) rigid barge platform with 8 catenary mooring lines. The width, length and height of the barge are 40 m, 40 m and 10 m,

respectively. The mass of the barge including ballast is 5,452,000 kg. The turbine's cut-in and cut-out wind speeds are 3 m/s and 25 m/s, respectively while the rated wind speed is 11.4 m/s.

We utilise NREL TurbSim [34] to generate stochastic, full-field, and turbulent wind flows for simulation studies. We use the IEC Kaimal spectral model (giving a good description of atmospheric turbulence [35]) with the IEC normal turbulence model (NTM) in TurbSim to determine wind spectra. For this purpose, we specify the mean hub-height longitudinal wind speed and turbulence intensity in the TurbSim input file. We use the standard IEC turbulence category A, B, or C (with A being the most turbulent) to specify the turbulence intensity. With the derived wind spectra, TurbSim uses an inverse Fourier transform to create the time series of wind speed vectors.

The NREL FAST code is used to simulate the dynamic responses of the NREL wind turbine models [36], which takes the aerodynamics, hydrodynamics, control and electrical (servo) dynamics, and structural (elastic) dynamics of offshore wind turbines into account. FAST includes InflowWind, AeroDyn, ElastoDyn, ServoDyn, HydroDyn, SubDyn, and MoorDyn modules. The dashed block in Figure 2 shows the schematic of FAST modules for the barge turbine [33]. InflowWind receives coordinates of various tower and blade nodes from AeroDyn. It computes undisturbed wind velocities (without interactions with the turbine) at these nodes through interpolating the time series of wind speed vectors from a stochastic inflow turbulence simulator (e.g., TurbSim), and outputs them to AeroDyn [37]. AeroDyn computes aerodynamic loads along blades and tower, and outputs them to ElastoDyn. ElastoDyn is a structural-dynamic model which outputs displacements, velocities, accelerations, and reaction loads to AeroDyn and ServoDyn. It simulates dynamics of the 6-DOF barge platform, and outputs barge motion & load data to MoorDyn which models the mooring system. ServoDyn includes control & actuator models for blade pitch, generator torque, nacelle yaw, etc. HydroDyn [38] receives barge motion data from ElastoDyn & MoorDyn, and calculates hydrodynamic loads on the barge and returns them back to ElastoDyn & MoorDyn. It allows for three approaches to calculate hydrodynamic loads, based on the potential-flow theory, the strip theory, and the combination of the two respectively. For the NREL barge, we use the combination of strip and potential-flow theories as recommended by Jonkman et al. [38]. The potential-flow theory provides hydrodynamic loads including excitation loads from incident waves, hydrostatic restoring loads, and added mass & damping loads associated with wave radiation. The strip theory produces viscous drag. The potential-flow method necessitates hydrodynamic coefficients which must be supplied by a separate numerical-panel code, e.g., WAMIT (Wave Analysis at MIT) used by FAST. HydroDyn incorporates several incident wave kinematics model to describe wave elevations (closely related to wave-excitation loads). We choose the JONSWAP spectrum to model irregular waves with no currents. This model depends on two user-prescribed parameters—the significant wave height and peak-spectral period of waves [14]. FAST can be interfaced with MATLAB/Simulink through a Simulink S-Function block. During simulations, this block calls the FAST Dynamic Library which is compiled as a dynamic-link-library (DLL) integrating all the FAST modules [36]. This enables flexible turbine modelling and control design in the Simulink environment.

3. TRANSFORMING THE NREL 5-MW BASELINE BARGE WIND TURBINE MODEL WITHIN FAST INTO AN HWT WITH A BTLCD RESERVOIR

In this section we transform the NREL 5-MW baseline barge wind turbine model within FAST (see Section 2) into a detailed aero-hydro-servo-elastic barge HWT model. To achieve this aim, we need to conduct the following three steps:

(a) Replace the gearbox drivetrain of the NREL baseline turbine model with a typical HST drivetrain as shown in Figure 1.

(b) Supersede the baseline torque and pitch controllers by their counterparts designed for the HWT.

(c) Incorporate coupled dynamics of the barge-reservoir system into FAST.

The steps (a) and (b) follow the similar procedures as our papers [39, 40] where we transformed an NREL 5-MW monopile wind turbine model within FAST into a monopile HWT, and thus are omitted here. In this paper we focus on step (c). We mention that here we use the same $\mathcal{H}_\infty$ loop-shaping design method for the torque controller to regulate the displacement of the hydraulic motor as in our paper [40], but design a new pitch controller—a gain-scheduled PI controller with the gains of the proportional and integral terms K_P and K_I scheduled by the pitch angle β:

$$K_P(\beta) = -\frac{1.0778}{1+\frac{\beta}{6.302336}}, K_I(\beta) = -\frac{0.3079}{1+\frac{\beta}{6.302336}}. \quad (1)$$

This scheduling implies that the idealised response of the rotor speed error will be like that of a second-order system with the natural frequency of 0.4 rad/s and the damping ratio of 0.7. Such a response was recommended by Jonkman [14] on the PI pitch control design for the NREL baseline barge wind turbine.

Wind Energ. 2018; **00**:1–?? © 2018 John Wiley & Sons, Ltd.
DOI: 10.1002/we
Prepared using weauth.cls

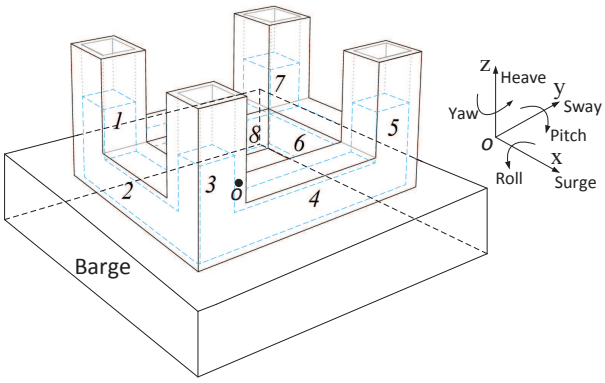

Figure 3. Barge with the BTLCD reservoir fixed on it.

3.1. BTLCD Reservoir Configuration on Top of the Barge of the Transformed NREL 5-MW HWT Model

In this section, we design a BTLCD reservoir on top of the barge of the transformed NREL 5-MW barge HWT model, see Figure 3. We adopt the BTLCD configuration proposed by Rozas et al. [32] for the reservoir. The barge has 6 motion DOFs in FAST including 3 translational DOFs (surge, sway and heave) and 3 rotational DOFs (roll, pitch and yaw), as shown in Figure 3 where $\mathbf{x}, \mathbf{y}, \mathbf{z}$ represents the set of orthogonal axes of a fixed inertial frame for these 6 DOFs. The $\mathbf{x}$-axis points in the nominal downwind direction, the $\mathbf{xy}$-plane designates the mean sea level (MSL) and the $\mathbf{z}$-axis points upward opposite to gravity along the undeflected tower's centreline when the barge is undisplaced. The $\mathbf{xy}$-plane coincides with the barge upper surface when the barge is undisplaced. The origin of $\mathbf{x}, \mathbf{y}, \mathbf{z}$ is denoted as O, which is the barge reference point defined in FAST. The 6 barge motion DOFs are defined about O on which the external loads act [14]. The BTLCD reservoir is composed of four vertical liquid columns (numbered 1, 3, 5 and 7) and four horizontal liquid columns (numbered 2, 4, 6 and 8). The columns numbered 1, 2, 3, 5, 6 and 7 form two TLCDs serving to damp barge pitch motions while the columns numbered 1, 7, 8, 3, 4 and 5 form two TLCDs to suppress barge roll motions.

We denote the rotational pitch, roll and yaw displacements of the barge as α, β and γ, respectively. Assume that $\mathbf{l}, \mathbf{s}, \mathbf{h}$ is the set of orthogonal axes of a coordinate system fixed on the barge so that it translates and rotates with the barge. It coincides with $\mathbf{x}, \mathbf{y}, \mathbf{z}$ when the barge is undisplaced. Jonkman [14] derived the transformation mapping from $\mathbf{x}, \mathbf{y}, \mathbf{z}$ to $\mathbf{l}, \mathbf{s}, \mathbf{h}$:

$$\begin{bmatrix}\mathbf{l} & \mathbf{s} & \mathbf{h}\end{bmatrix}^T = \mathbf{T}\begin{bmatrix}\mathbf{x} & \mathbf{y} & \mathbf{z}\end{bmatrix}^T \tag{2}$$

where transformation matrix

$$\mathbf{T} = \frac{1}{\Delta_3}\begin{bmatrix} \beta^2\Delta_2 + \alpha^2 + \gamma^2 & \gamma\Delta_1 + \beta\alpha\left(\Delta_2 - 1\right) & -\alpha\Delta_1 + \gamma\beta\left(\Delta_2 - 1\right) \\ -\gamma\Delta_1 + \alpha\beta\left(\Delta_2 - 1\right) & \beta^2 + \alpha^2\Delta_2 + \gamma^2 & \beta\Delta_1 + \alpha\gamma\left(\Delta_2 - 1\right) \\ \alpha\Delta_1 + \beta\gamma\left(\Delta_2 - 1\right) & -\beta\Delta_1 + \alpha\gamma\left(\Delta_2 - 1\right) & \alpha^2 + \beta^2 + \gamma^2\Delta_2 \end{bmatrix} \tag{3}$$

where

$$\Delta_1 = \alpha^2 + \beta^2 + \gamma^2,\ \Delta_2 = \sqrt{1 + \Delta_1},\ \Delta_3 = \Delta_1\Delta_2. \tag{4}$$

The rigid barge and the BTLCD reservoir are symmetric with respect to the $\mathbf{lh}$- and $\mathbf{sh}$-planes.

Figure 4 is the three-view drawing of the BTLCD reservoir. A_x and L_x are the cross-section area and length of the horizontal columns numbered 2 and 6, respectively. A_y and L_y are the cross-section area and length of the horizontal columns numbered 4 and 8, respectively. A_v and L_v are the cross-section area and length (when the liquid is undisplaced) of all vertical columns. $u_k (k = 1, 2, \ldots, 8)$ is the liquid displacement in the column numbered k relative to the BTLCD reservoir. The liquid displacement in a vertical column can be related to the liquid displacements in the adjacent horizontal columns, e.g.,

$$u_1 = -\left(r_x u_2 + r_y u_8\right), \tag{5}$$

where

$$r_x = A_x/A_v, \quad r_y = A_y/A_v \tag{6}$$

are the cross-section area ratios. There exists an orifice within each horizontal column of the BTLCD reservoir which generates a head loss. The head loss coefficient in columns numbered 2 and 6 is denoted as η_l. The head loss coefficient in columns numbered 4 and 8 is denoted as η_s. The effective mass and natural frequency of the liquid in columns numbered

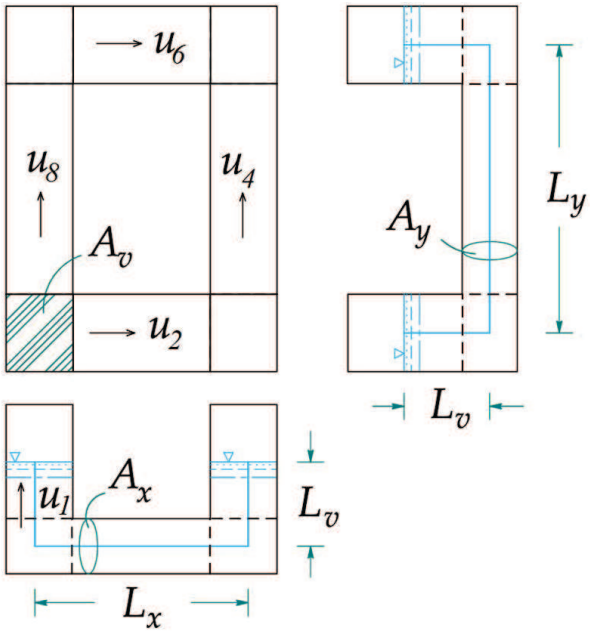

Figure 4. Three-view drawing of the BTLCD reservoir.

1, 2, 3, 5, 6 and 7 which serves to damp barge pitch motions, are

$$M_{lp} = \rho_l A_v \left(4L_v + 2r_x L_x\right), \omega_{lp} = \sqrt{2g/L_{el}}, \tag{7}$$

respectively, where $\rho_l = 917$ kg/m^3 is the liquid density, g is the acceleration of gravity and $L_{el} = 2L_v + L_x/r_x$ is the equivalent length of the liquid for suppressing barge pitch motions. The effective mass and natural frequency of the liquid in columns numbered 1, 7, 8, 3, 4 and 5 (which serve to damp barge roll motions), are

$$M_{lr} = \rho_l A_v \left(4L_v + 2r_y L_y\right), \omega_{lr} = \sqrt{2g/L_{es}}, \tag{8}$$

respectively, where $L_{es} = 2L_v + L_y/r_y$ is the equivalent length of the liquid for mitigating barge roll motions. The total mass of the liquid in the BTLCD reservoir is

$$M_l = \rho_l A_v \left(4L_v + 2r_x L_x + 2r_y L_y\right). \tag{9}$$

3.2. Incorporating Coupled Dynamics of the Barge-reservoir System into the FAST Code

The FAST code uses Kane's dynamics (a direct result of Newton's law of motion) to obtain equations of motions (EOMs) of a wind turbine [14]. The time-domain EOMs of the whole baseline barge wind turbine are

$$M_{ij}\ddot{q}_j = f_i\left(\dot{\mathbf{q}}, \mathbf{q}\right), \tag{10}$$

where $\mathbf{q}$ is the set of turbine DOFs, q_j is the jth DOF, and M_{ij} is the (i, j)th component of the coefficient matrix for the accelerations of DOFs. f_i is the forcing function associated with q_i, which depends on $\mathbf{q}$ and $\dot{\mathbf{q}}$.

The dynamics of the BTLCD reservoir interact with the barge surge, sway, heave, pitch, roll and yaw DOFs (denoted as $q_1, q_2, \ldots, q_6$, respectively). Thus, the extra forcing function $f_m^r (m = 1, 2, \ldots, 6)$ (which depends on $u_1, u_2, \ldots, u_8, q_1, q_2, \ldots, q_6$ along with their first and second derivatives) should be added to f_m in (10) after we incorporate the BTLCD. We derive the EOMs of the BTLCD reservoir and f_m^r using Lagrange's equations, which are the scalar equivalents of Newton's law of motion. The kinetic energy of the BTLCD reservoir is

$$T_l = \sum_{k=1}^{8} T_k, \tag{11}$$

Wind Energ. 2018; **00**:1–?? © 2018 John Wiley & Sons, Ltd.
DOI: 10.1002/we
Prepared using weauth.cls

where T_k is the kinetic energy of the liquid column numbered k, where

$$T_1 = \frac{1}{2}\rho_l A_v \int_0^{L_v-\left(r_x u_2+r_y u_8\right)} \mathbf{v}_1^2 \mathrm{d}h,\ T_2 = \frac{1}{2}\rho_l r_x A_v \int_{-Lx/2}^{Lx/2} \mathbf{v}_2^2 \mathrm{d}l, \tag{12}$$

in which h and l are respectively the coordinates of the liquid particle along the $\mathbf{h}$- and $\mathbf{l}$-axes. $\mathbf{v}_1$ and $\mathbf{v}_2$ are the velocities of any liquid particle in columns numbered 1 and 2 relative to the inertial frame:

$$\begin{aligned}
\mathbf{v}_1 &= \dot{q}_1\mathbf{x}+\dot{q}_2\mathbf{y}+\dot{q}_3\mathbf{z}+\dot{u}_1\mathbf{h}+\left(\dot{\alpha}\mathbf{y}+\dot{\beta}\mathbf{x}+\dot{\gamma}\mathbf{z}\right)\times\left(-\tfrac{L_x}{2}\mathbf{l}-\tfrac{L_y}{2}\mathbf{s}+h\mathbf{h}\right)\\
&= \left[\dot{q}_1+\dot{u}_1\mathbf{T}(3,1)+\dot{\alpha}\left(h\mathbf{T}(3,3)-\tfrac{L_x}{2}\mathbf{T}(1,3)-\tfrac{L_y}{2}\mathbf{T}(2,3)\right)+\dot{\gamma}\left(-h\mathbf{T}(3,2)+\tfrac{L_x}{2}\mathbf{T}(1,2)+\tfrac{L_y}{2}\mathbf{T}(2,2)\right)\right]\mathbf{x}+\\
&\left[\dot{q}_2+\dot{u}_1\mathbf{T}(3,2)+\dot{\beta}\left(-h\mathbf{T}(3,3)+\tfrac{L_x}{2}\mathbf{T}(1,3)+\tfrac{L_y}{2}\mathbf{T}(2,3)\right)+\dot{\gamma}\left(h\mathbf{T}(3,1)-\tfrac{L_x}{2}\mathbf{T}(1,1)-\tfrac{L_y}{2}\mathbf{T}(2,1)\right)\right]\mathbf{y}+\\
&\left[\dot{q}_3+\dot{u}_1\mathbf{T}(3,3)+\dot{\alpha}\left(-h\mathbf{T}(3,1)+\tfrac{L_x}{2}\mathbf{T}(1,1)+\tfrac{L_y}{2}\mathbf{T}(2,1)\right)+\dot{\beta}\left(h\mathbf{T}(3,2)-\tfrac{L_x}{2}\mathbf{T}(1,2)-\tfrac{L_y}{2}\mathbf{T}(2,2)\right)\right]\mathbf{z},\\
\mathbf{v}_2 &= \dot{q}_1\mathbf{x}+\dot{q}_2\mathbf{y}+\dot{q}_3\mathbf{z}+u_2\mathbf{l}+\left(\dot{\alpha}\mathbf{y}+\dot{\beta}\mathbf{x}+\dot{\gamma}\mathbf{z}\right)\times\left(l\mathbf{l}-\tfrac{L_y}{2}\mathbf{s}\right)\\
&= \left[\dot{q}_1+\dot{u}_2\mathbf{T}(1,1)+\dot{\alpha}\left(l\mathbf{T}(1,3)-\tfrac{L_y}{2}\mathbf{T}(2,3)\right)+\dot{\gamma}\left(-l\mathbf{T}(1,2)+\tfrac{L_y}{2}\mathbf{T}(2,2)\right)\right]\mathbf{x}+[\dot{q}_2+\dot{u}_2\mathbf{T}(1,2)+\\
&\dot{\beta}\left(-l\mathbf{T}(1,3)+\tfrac{L_y}{2}\mathbf{T}(2,3)\right)+\dot{\gamma}\left(l\mathbf{T}(1,1)-\tfrac{L_y}{2}\mathbf{T}(2,1)\right)\Big]\mathbf{y}+\left[\dot{q}_3+\dot{u}_2\mathbf{T}(1,3)+\dot{\alpha}\left(-l\mathbf{T}(1,1)+\tfrac{L_y}{2}\mathbf{T}(2,1)\right)+\right.\\
&\left.\dot{\beta}\left(l\mathbf{T}(1,2)-\tfrac{L_y}{2}\mathbf{T}(2,2)\right)\right]\mathbf{z},
\end{aligned} \tag{13}$$

where $\mathbf{T}$ is given in (3). $T_3, T_4, \ldots, T_8$ can be derived in a similar way.

We choose the point of zero potential energy to be the origin O of $\mathbf{x}, \mathbf{y}, \mathbf{z}$ as shown in Figure 3. The potential energy of the BTLCD reservoir is

$$V_l = M_l g q_3 + \sum_{k=1}^{8} V_k. \tag{14}$$

V_k is the potential energy of the liquid column numbered k relative to the barge reference point O, where

$$\begin{aligned}
&V_1 = \rho_l A_v g\left(L_v+u_1\right)\left[-\tfrac{L_x}{2}\mathbf{l}-\tfrac{L_y}{2}\mathbf{s}+\tfrac{L_v+u_1}{2}\mathbf{h}\right]\mathbf{z}\\
&= \rho_l A_v g\left(L_v+u_1\right)\left[-\tfrac{L_x}{2}\mathbf{T}(1,3)-\tfrac{L_y}{2}\mathbf{T}(2,3)+\tfrac{L_v+u_1}{2}\mathbf{T}(3,3)\right],\\
&V_2 = V_4 = V_6 = V_8 = 0.
\end{aligned} \tag{15}$$

V_3, V_5 and V_7 can be derived in a similar way.

The total kinetic and potential energies of the HWT are respectively

$$T_t = T_l + T_b,\ V_t = V_l + V_b, \tag{16}$$

where T_b and V_b are the kinetic and potential energies of the HWT (except the BTLCD reservoir), respectively. Using Lagrange's equations, the EOMs of the whole HWT are

$$\frac{\mathrm{d}}{\mathrm{d}t}\left(\frac{\partial \mathcal{L}}{\partial \dot{q}_i}\right)-\frac{\partial \mathcal{L}}{\partial q_i} = f_{Li},\ \mathcal{L} = T_t - V_t, \tag{17}$$

where f_{Li} is the non-conservative force acting on the DOF q_i, where $i = 1, 2, \ldots, n+4$ (n is the number of turbine DOFs without the BTLCD reservoir). The extra DOFs $q_{n+1} - q_{n+4}$ are equivalent to u_2, u_4, u_6 and u_8, respectively. They represent liquid displacements in four horizontal columns relative to the reservoir. Note that dynamics associated with the terms $\frac{\mathrm{d}}{\mathrm{d}t}\left(\frac{\partial T_b}{\partial \dot{q}_j}\right)$, $\frac{\mathrm{d}}{\mathrm{d}t}\left(\frac{\partial V_b}{\partial \dot{q}_j}\right)$, $\frac{\partial T_b}{\partial q_j}$, $\frac{\partial V b}{\partial q_j}$ and $f_{L1}, f_{L2}, \ldots, f_{Ln}$ have already been contained in the FAST code. Hence, f_m^r $(m = 1, 2, \ldots, 6)$ is

$$f_m^r = \frac{\partial\left(T_l - V_l\right)}{\partial q_m}-\frac{\mathrm{d}}{\mathrm{d}t}\left(\frac{\partial\left(T_l - V_l\right)}{\partial \dot{q}_m}\right). \tag{18}$$

The non-conservative forces $f_{L(n+1)} - f_{L(n+4)}$ acting on the DOFs $q_{n+1} - q_{n+4}$ are the damping forces induced by the head loss of flow generated by the orifice within the four horizontal columns of the BTLCD reservoir, which are

$$\begin{aligned}
f_{L(n+1)} &= -\tfrac{1}{2}\rho_l A_v r_x \eta_l \dot{q}_{n+1}\left|\dot{q}_{n+1}\right|,\\
f_{L(n+2)} &= -\tfrac{1}{2}\rho_l A_v r_y \eta_s \dot{q}_{n+2}\left|\dot{q}_{n+2}\right|,\\
f_{L(n+3)} &= -\tfrac{1}{2}\rho_l A_v r_x \eta_l \dot{q}_{n+3}\left|\dot{q}_{n+3}\right|,\\
f_{L(n+4)} &= -\tfrac{1}{2}\rho_l A_v r_y \eta_s \dot{q}_{n+4}\left|\dot{q}_{n+4}\right|.
\end{aligned} \tag{19}$$

The EOMs of the BTLCD reservoir are then derived as

$$\frac{\mathrm{d}}{\mathrm{d}t}\left(\frac{\partial\left(T_l - V_l\right)}{\partial \dot{q}_{n+w}}\right) - \frac{\partial\left(T_l - V_l\right)}{\partial q_{n+w}} = f_{L(n+w)}, \tag{20}$$

where $w = 1, 2, 3, 4$.

Based on (20), we create the Simulink model of the BTLCD reservoir, which is coupled with the FAST code via the FAST/Simulink interface (see Section 2 and Figure 2). Using the input $\mathbf{U} = \begin{bmatrix} q_1 & q_2 & \cdots & q_6 & \dot{q}_1 & \dot{q}_2 & \cdots & \dot{q}_6 & \ddot{q}_1 & \ddot{q}_2 & \cdots & \ddot{q}_6 \end{bmatrix}$ (representing platform dynamics) from FAST, this Simulink model computes $u_1, u_2, \ldots, u_8$, and their first and second derivatives. It also calculates f_m^r $(m = 1, 2, \ldots, 6)$ (18) which is outputted to FAST and added to f_m in (10) for the computation of $\mathbf{U}$.

4. OPTIMISING THE PARAMETERS OF THE BTLCD RESERVOIR FOR MITIGATING BARGE PITCH AND ROLL MOTIONS

The BTLCD reservoir is designed to suppress the barge pitch and roll motions. Since the fore-aft direction suffers the largest loading from winds and waves, we first optimise the reservoir parameters based on a simplified mathematical model Σ_p describing the fore-aft (pitch) motions of the turbine-reservoir system. Then we optimise the remaining reservoir parameters based on a simplified model Σ_r describing the side-to-side (roll) motions. The FAST code employs the barge kinematics and kinetics modelling, the barge hydrodynamics modelling, and the modelling of catenary mooring lines to simulate barge dynamics [14]. Because the first tower fore-aft and side-to-side bending modes dominate the dynamic responses of the barge wind turbine tower and the largest deflections for both modes occur at the tower top [41], either Σ_p or Σ_r can be treated as an inverted pendulum on a barge platform.

We create Σ_p by taking into account 3 DOFs: the liquid displacement q_{n+1}/q_{n+3} (u_2/u_6 in Figure 4) in the horizontal column numbered 2/6 relative to the reservoir (note that $q_{n+1} = q_{n+3}$ when only considering pitch motions of the turbine-reservoir system), the rotational pitch displacement of the pendulum tower from the $\mathbf{z}$-axis denoted as q_7, and the barge pitch displacement DOF q_4. The kinetic and potential energies of Σ_p are respectively

$$\begin{aligned} T_{op} &= \tfrac{1}{2} I_{tp} \dot{q}_7^2 + \tfrac{1}{2} I_{bp} \dot{q}_4^2 + T_{lp}, \\ V_{op} &= \tfrac{1}{2} k_{tp} \left(q_7 - q_4\right)^2 + \tfrac{1}{2}\left(C_{hs} + C_{ml}\right) q_4^2 + m_t g L_t \cos q_7 - m_p g L_p \cos q_4 + V_{lp}, \end{aligned} \tag{21}$$

where I_{tp} is the pitch inertia of the tower & RNA (rotor nacelle assembly) and I_{bp} is the barge pitch inertia. Both of them are about the barge reference point O. C_{hs} is the hydrostatic pitch restoring coefficient and C_{ml} is the linearised pitch restoring coefficient from mooring lines. m_t and k_{tp} are the total mass and equivalent pitch restoring coefficient of the tower & RNA, respectively. m_p is the mass of the barge, L_t is the distance from the mass centre of the tower & RNA to O, and L_p is the distance from the mass centre of the barge to O. T_{lp} and V_{lp} are respectively T_l and V_l of (11) and (14) when setting $q_1, q_2, q_3, q_5, q_6, u_4\,(q_{n+2}), u_8\,(q_{n+4})$ and their first derivatives to be zero, and substituting u_6 and $\dot{u}_6$ with u_2 and $\dot{u}_2$. Applying the Lagrange's equation approach, we obtain Σ_p

$$\frac{\mathrm{d}}{\mathrm{d}t}\left(\frac{\partial \mathcal{L}_{op}}{\partial \dot{q}_r}\right) - \frac{\partial \mathcal{L}_{op}}{\partial q_r} = f_{Lr},\ \mathcal{L}_{op} = T_{op} - V_{op}, \tag{22}$$

where $r = 4, 7, n+1$. $f_{L(n+1)}$ is given in (19), and

$$\begin{aligned} f_{L4} &= -A_{rad}\ddot{q}_4 - \left(B_{rad} + B_{vis}\right)\dot{q}_4 + d_{tp}\left(\dot{q}_7 - \dot{q}_4\right) + M_w, \\ f_{L7} &= -d_{tp}\left(\dot{q}_7 - \dot{q}_4\right) + F_a L_{hh}, \end{aligned} \tag{23}$$

where A_{rad} and B_{rad} are the added pitch inertia and the pitch damping coefficient associated with hydrodynamic radiation, respectively. B_{vis} is the linearised pitch damping coefficient associated with hydrodynamic viscous drag. M_w is the total wave-excitation pitch moment from diffraction applied at O. d_{tp} is the equivalent pitch damping coefficient of the tower & RNA. L_{hh} is the hub height and F_a is the aerodynamic rotor thrust acting on the hub. F_a can be described by a first-order Taylor series expansion [14]:

$$F_a = F_{a0} - \frac{\partial F_a}{\partial V_a} L_{hh} \dot{q}_7, \tag{24}$$

where V_a is the steady hub-height wind speed and F_{a0} is the aerodynamic rotor thrust at V_a. $\frac{\partial F_a}{\partial V_a}$ can be derived through FAST linearisation at V_a [14]. In (21) and (23), m_t, m_p and L_{hh} are given by Jonkman [14]. We obtain I_{tp}, I_{bp}, L_t and L_p using the Aggregate Mass tool in ADAMS (Automatic Dynamic Analysis of Mechanical Systems) based on the ADAMS wind turbine datasets generated by the FAST-to-ADAMS preprocessor [36]. C_{hs}, A_{rad} and B_{rad} are respectively

DOI: 10.1002/we
Prepared using weauth.cls

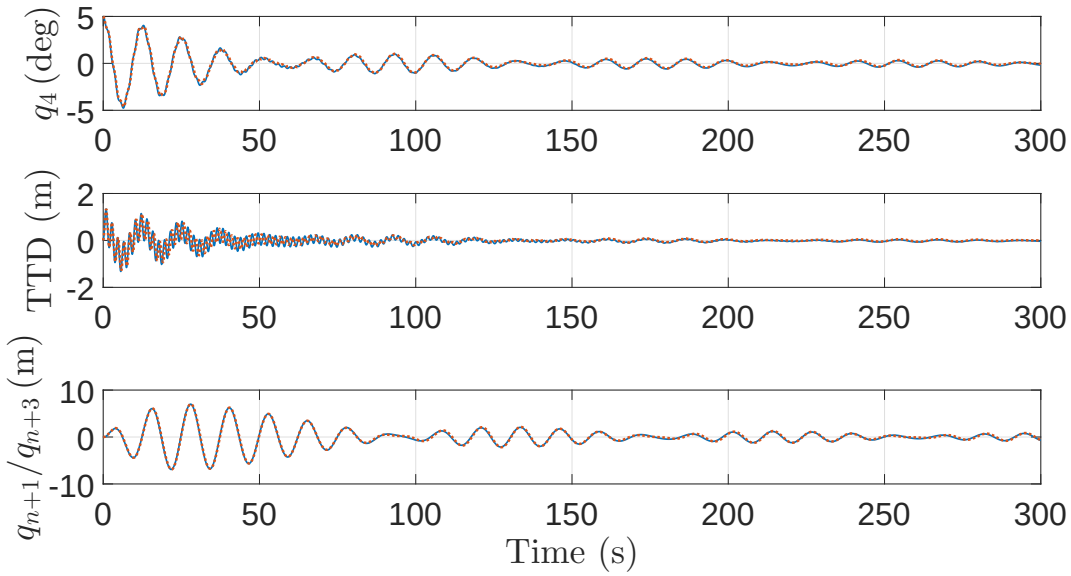

Figure 5. Barge pitch displacements q_4, tower-top displacements (TTD), and liquid displacements q_{n+1}/q_{n+3} obtained from simulations on the transformed NREL 5-MW barge HWT model within the FAST code (blue solid lines) and the simplified turbine-reservoir model Σ_p (22) (red dotted lines).

derived from the hydrostatic restoring matrix, hydrodynamic-added-mass and hydrodynamic-damping matrices created by WAMIT (Wave Analysis at MIT) which is the hydrodynamic preprocessor for FAST. We compute k_{tp} and d_{tp} from a FAST linearisation analysis by only activating the first tower fore-aft bending DOF. B_{vis} and C_{ml} are derived from a FAST linearisation analysis by only activating the barge pitch displacement DOF. The loading data F_{a0} and M_w can be extracted from output data generated by simulations on the transformed NREL HWT model within FAST. The parameters of the BTLCD reservoir in Σ_p (22) are $L_x,\ L_v,\ r_x,\ \eta_l,\ \rho_l A_v$ and $r_y L_y$. From (7) and (8), we get

$$\rho_l A_v = \frac{M_{lp}}{4L_v + 2r_x L_x} = \frac{M_{lr}}{4L_v + 2r_y L_y}. \tag{25}$$

We denote the two mass ratios as

$$\mu_p = \frac{M_{lp}}{M_{tb}},\ \mu_r = \frac{M_{lr}}{M_{tb}}, \tag{26}$$

where $M_{tb} = 6149460.25$ kg is the total mass of the HWT except the reservoir. Combining (25) with (26), we obtain

$$r_y L_y = \frac{2L_v\left(\mu_r - \mu_p\right) + \mu_r r_x L_x}{\mu_p}. \tag{27}$$

Since large values of the mass ratios μ_p and μ_r are practically infeasible [42], we set $\mu_p = 6\%$ and $\mu_r = 4\%$. We specify $\mu_p > \mu_r$ to provide more damping in the fore-aft direction than in the side-to-side direction. The BTLCD parameters to be optimised are:

$$\mathbf{x}_{op} = \begin{bmatrix} L_x & L_v & r_x & \eta_l \end{bmatrix}. \tag{28}$$

We now verify Σ_p (22) against the transformed NREL 5-MW barge HWT model through structural simulations. We let both models oscillate freely from an initial barge pitch angle of 5°. Then we set F_a and M_w in (23) to be 0, and employ an ODE (ordinary differential equation) solver in Matlab to simulate the dynamics of Σ_p. Equivalently for the transformed NREL HWT model, we only enable its barge pitch displacement DOF and the first tower fore-aft bending DOF, and disable the wind & wave effects. Figure 5 shows the simulation results of the barge pitch displacements q_4, tower-top displacements (TTD), and liquid displacements q_{n+1}/q_{n+3} on both models. Clearly they agree very well.

Now we optimise the BTLCD reservoir parameters $\mathbf{x}_{op}$ in (28) based on Σ_p. The barge pitch mode has a natural frequency of about 0.0863 Hz (0.542 rad/s) [14]. Thus, the waves with peak spectral periods between 10 s and 15 s are most likely to excite that mode, causing large barge pitch motions. Besides, barge pitch motions grow as the wind speed increases. Therefore, our optimisation problem is to find an optimal $\mathbf{x}_{op}$ to minimise the maximal barge pitch displacement q_4 under specific loading conditions. We choose the excitation loadings of Σ_p based on FAST simulation data of the transformed NREL 5-MW barge HWT. We set the value of F_{a0} in (24) as the average aerodynamic rotor thrust of the

transformed NREL HWT under a steady hub-height wind speed of 24 m/s (recall that the cut-out wind speed is 25 m/s) with all the tower and barge DOFs disabled. We generate eleven 100-second time-series for M_w (wave-excitation pitch moment from diffraction) in (23), through the FAST simulations on the transformed NREL HWT model under the excitations of 11 irregular waves. As mentioned in Section 2, the waves are modelled based on the JONSWAP spectrum and generated by the HydroDyn module in FAST, with the peak-spectral periods ranging from 10 s to 15 s in steps of 0.5 s. All the eleven waves have a same significant wave height of 5.5 m. Next we conduct 11 simulations on Σ_p using these M_w and F_{a0}, among which we obtain the maximal barge pitch displacement q_4. We utilise multistart optimisation to search for the optimal $\mathbf{x}_{op}$ (28). More specifically, we run the MATLAB sequential quadratic programming (SQP) algorithm *fmincon* from 40 randomly selected starting points within the bounds on the design parameters to obtain a local minimum. To ensure that the liquid remains in the four vertical columns of the BTLCD reservoir and that the length of horizontal columns does not exceed the length of the barge (40 m), we enforce a constraint:

$$r_x \cdot \max |q_{n+1}| \leq S_F L_v, \tag{29}$$

where $r_x \cdot \max |q_{n+1}|$ is the maximal liquid displacement occurring in the vertical columns during all the eleven simulations. We set $S_F = 0.8$ to leave a margin in the vertical column, which may be used for damping barge roll motions. Besides, we set $1\text{m} \leq L_x \leq 40\text{m}$, $1\text{m} \leq L_v \leq 7\text{m}$, $0.1 \leq r_x \leq 10$ and $0 \leq \eta_l \leq 10$. The first two constraints are set to take into account the fact that the length of horizontal columns should not exceed the barge length (40 m) and that the height of the reservoir should not be too large. Finally we obtain the optimal $\mathbf{x}_{op}$:

$$\mathbf{x}_{op} = \begin{bmatrix} 30.15\text{m} & 7\text{m} & 0.51 & 2.24 \end{bmatrix}, \tag{30}$$

from which we get that the natural frequency of the liquid serving to damp barge pitch motions is 0.5166 rad/s according to (7), which is 95.31% of the barge pitch modal frequency (0.542 rad/s).

Similarly we get the following optimal values for the remaining parameters of the BTLCD reservoir based on the simple model Σ_r which describes the side-to-side (roll) motions of the turbine-reservoir system:

$$\mathbf{x}_{or} = \begin{bmatrix} L_y & r_y & \eta_s \end{bmatrix} = \begin{bmatrix} 18.43\text{m} & 0.3 & 1.46 \end{bmatrix}. \tag{31}$$

We mention that $r_y L_y$ is a constant after $\mathbf{x}_{op}$ (28) is determined, according to (27). Therefore, we have actually optimised the last two parameters. And during our optimisation, we have set $r_y \max |q_{n+2}| \leq 0.2 L_v$, $1\text{m} \leq L_y \leq 40\text{m}$ and $0 \leq \eta_s \leq 10$, where q_{n+2} (u_4) is the liquid displacement in the horizontal column numbered 4 relative to the BTLCD reservoir. Based on the parameters in (31), we get that the natural frequency of the liquid serving to damp barge roll motions is 0.5098 rad/s according to (8), which is 94.05% of the barge roll modal frequency (0.542 rad/s). Using (6), (25), (26), (30), and (31), we get the optimal BTLCD dimensions as follows. The cross-section area and length of the horizontal columns numbered 2 and 6 (see Figures 3 and 4) are $A_x = 3.49\ \text{m}^2$ and $L_x = 30.15$ m. The cross-section area and length of the horizontal columns numbered 4 and 8 are $A_y = 2.05\ \text{m}^2$ and $L_y = 18.43$ m. The cross-section area and length (when the liquid is undisplaced) of all the vertical columns are $A_v = 6.85\ \text{m}^2$ and $L_v = 7$ m. The optimal head loss coefficient in columns numbered 2 and 6 is $\eta_l = 2.24$ while the optimal head loss coefficient in columns numbered 4 and 8 is $\eta_s = 1.46$. The total mass of the liquid in the BTLCD reservoir is 438552 kg following (9), which is 6.66% of the HWT mass.

5. SIMULATION STUDY

We carry out FAST simulations based on the transformed NREL 5-MW barge HWT model in both cases without and with the BTLCD configuration whose optimal parameters are given in (30) and (31). Recall that this simulation model is developed following steps (a)–(c) at the beginning of Section 3. Here we conduct the simulations under two types of extreme events and two types of normal events. The two extreme events are for the tower-base fore-aft bending moment (Event E.1) and the side-to-side bending moment (Event E.2) respectively, which were recorded in the report [14]. The wind conditions in all the events are generated based on the IEC Kaimal Spectral Model with NTM in TurbSim (see Section 2). For Events E.1 and E.2, the mean hub-height longitudinal wind speeds are 22 m/s and 24 m/s respectively, and the turbulence intensity is category B. For the two normal events (Event N.1 and Event N.2), the mean hub-height longitudinal wind speeds are 9 m/s (below-rated) and 18 m/s (above-rated) respectively, and the turbulence intensity is category A. The wave conditions in all the events are generated by the HydroDyn module which is integrated into FAST based on the JONSWAP spectrum (see Section 2). For Events E.1 and E.2, the peak-spectral periods of the incident waves are 13.4 s and 15.5 s respectively, with the significant wave heights being 4.7 m and 5.5 m. For Events N.1 and N.2, the peak-spectral periods of the incident waves are 12 s and 11 s respectively, with the significant wave heights being 2 m and 4.5 m.

Wind Energ. 2018; **00**:1–?? © 2018 John Wiley & Sons, Ltd.
DOI: 10.1002/we
Prepared using weauth.cls

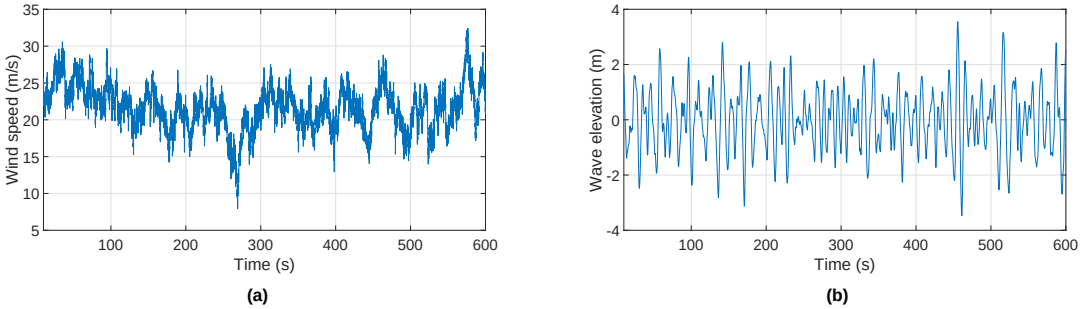

Figure 6. The hub-height longitudinal wind speed and wave elevation in the extreme event for the tower-base fore-aft bending moment.

Figures 6 and 9 show the hub-height longitudinal wind speeds and the wave elevations in the two extreme events (Events E.1 and E.2). As shown in Figures 7 and 10, in both events, the barge pitch and roll displacements of the HWT with the BTLCD configuration are much smaller than the cases without the BTLCD configuration, which results in less fluctuations in the rotor speed and generator power. Due to the BTLCD configuration, the standard deviations (SDs) of the barge pitch and roll displacements reduce by 21.36% and 42.42% respectively in Event E.1, and decrease by 22.61% and 30.51% respectively in Event E.2. The absolute peaks of the barge pitch and roll displacements reduce by 11.25% and 39.34% respectively in Event E.1, and decrease by 14.66% and 26.95% respectively in Event E.2. Besides, the SDs of the rotor speed and the generator power decrease by 12.05% and 14.98% respectively in Event E.1, and decrease by 14.45% and 12.38% respectively in Event E.2. It is clear from Figures 8 and 11 that the liquid remains in the BTLCD reservoir during these simulations.

Table I summarises the fore-aft and side-to-side damage equivalent loads (DEQLs) at the tower base in both cases with and without the BTLCD configuration, during the above simulations for the two extreme events. We employed MLife [43] to calculate these DEQL using the time-series of the tower-base bending moment based on a rainflow counting algorithm. The tower-base DEQL reduction ratios due to the BTLCD configuration in Table I demonstrates that the optimal BTLCD reservoir can effectively reduce the tower loads.

Figures 12 and 15 show the hub-height longitudinal wind speeds and the wave elevations in the two normal events (Events N.1 and N.2). As illustrated in Figures 13 and 16, in both events, the barge pitch and roll displacements of the HWT with the BTLCD configuration are much smaller than the cases without the BTLCD configuration, which results in less fluctuations in the rotor speed and generator power. Due to the BTLCD configuration, the SDs of the barge pitch and roll displacements reduce by 18.78% and 36.14% respectively in Event N.1 where the mean hub-height longitudinal wind speed is 9 m/s, and decrease by 22.95% and 34.86% respectively in Event N.2 where the mean hub-height longitudinal wind speed is 18 m/s. The absolute peaks of the barge pitch and roll displacements reduce by 13.22% and 28.85% respectively in Event N.1, and decrease by 19.32% and 25.16% respectively in Event N.2. In addition, the SDs of the rotor speed and the generator power decrease by 13.30% and 14.71% respectively in Event N.2. The BTLCD reservoir does not change the SDs of the rotor speed and generator power very much in Event N.1 because in this event the wind speed is below-rated during most of the simulation period (see Figure 12a) and therefore the turbine is controlled to capture maximum power rather than track a fixed rotor speed and a fixed rotor power. It is clear from Figures 14 and 17 that the liquid remains in the BTLCD reservoir during these simulations.

Table II summarises the fore-aft and side-to-side DEQLs at the tower base in both cases with and without the BTLCD configuration, during the above simulations for the two normal events. The tower-base DEQL reduction ratios due to the BTLCD configuration in Table II demonstrates that the optimal BTLCD reservoir can effectively reduce the tower loads.

It is noticeable from Figures 7, 10, 13, and 16 that the BTLCD is more effective in damping the barge roll (side-to-side) oscillations than the pitch (fore-aft) oscillations. A similar phenomenon was observed by Stewart and Lackner [44] where a TMD (tuned mass damper) system was configured in the NREL barge to mitigate tower-base damage loads. We borrow their explanations. This phenomenon is most likely because there is no direct wind or wave loading in the side-to-side direction and the excitation is mainly due to DOF coupling. This means the barge side-to-side (roll) oscillations have most of its energy at the barge roll modal frequency. By contrast, the barge fore-aft (pitch) oscillations are excited by both the structural vibrations (corresponding to the barge pitch model frequency) and the broadband wind and wave loadings. Since the BTLCD is tuned to the modal frequencies of the barge pitch and roll modes, it is more effective in the side-to-side direction.

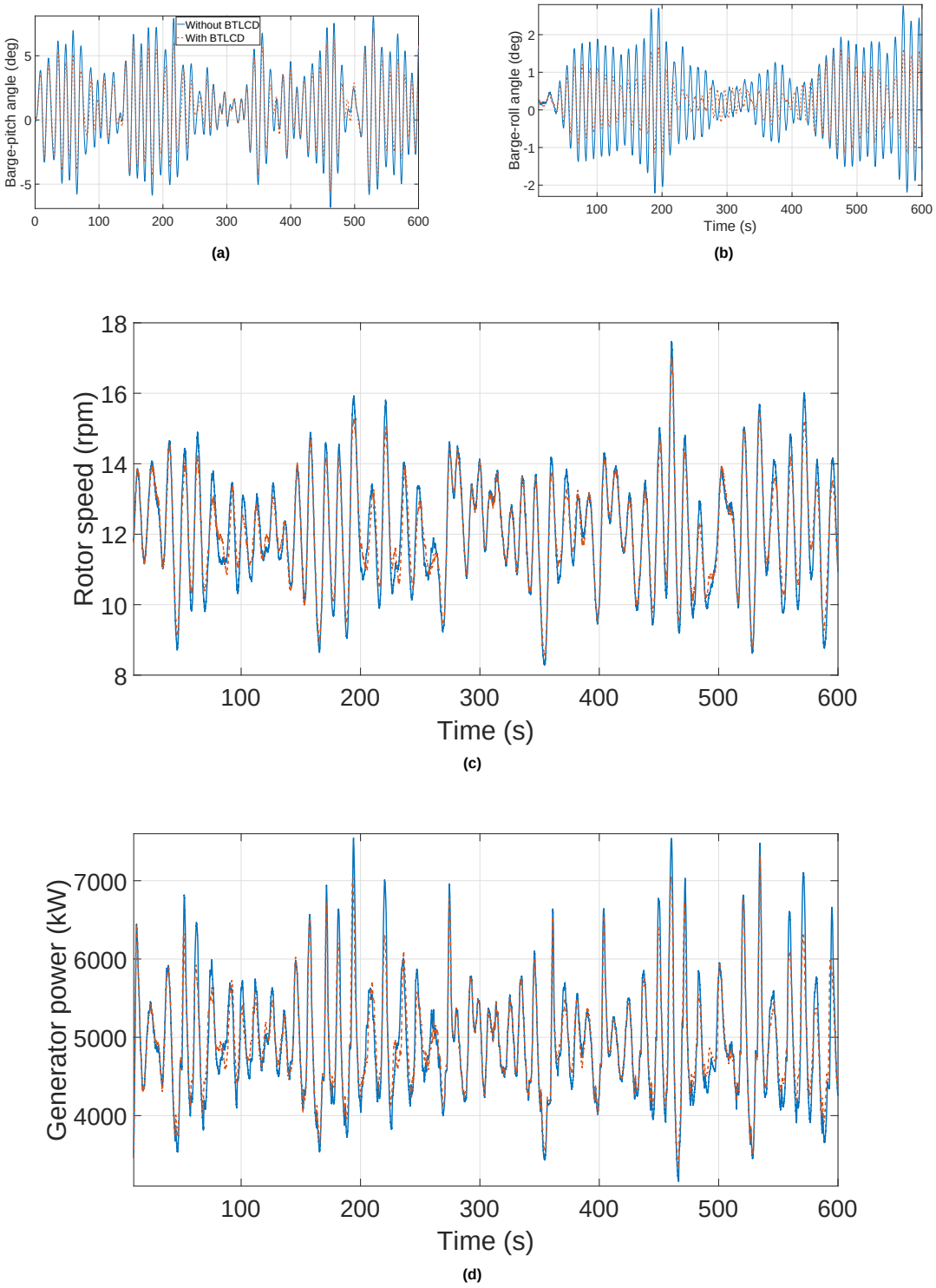

Figure 7. Simulations results for the transformed NREL 5-MW barge HWT model in the cases without (blue solid lines) and with (red dash lines) the BTLCD configuration, in the extreme event for the tower-base fore-aft bending moment. Figure 7a, 7b, 7c and 7d depict the barge pitch and roll displacements, the rotor speed and the generator power,respectively.

Wind Energ. 2018; **00**:1–?? © 2018 John Wiley & Sons, Ltd.
DOI: 10.1002/we
Prepared using weauth.cls

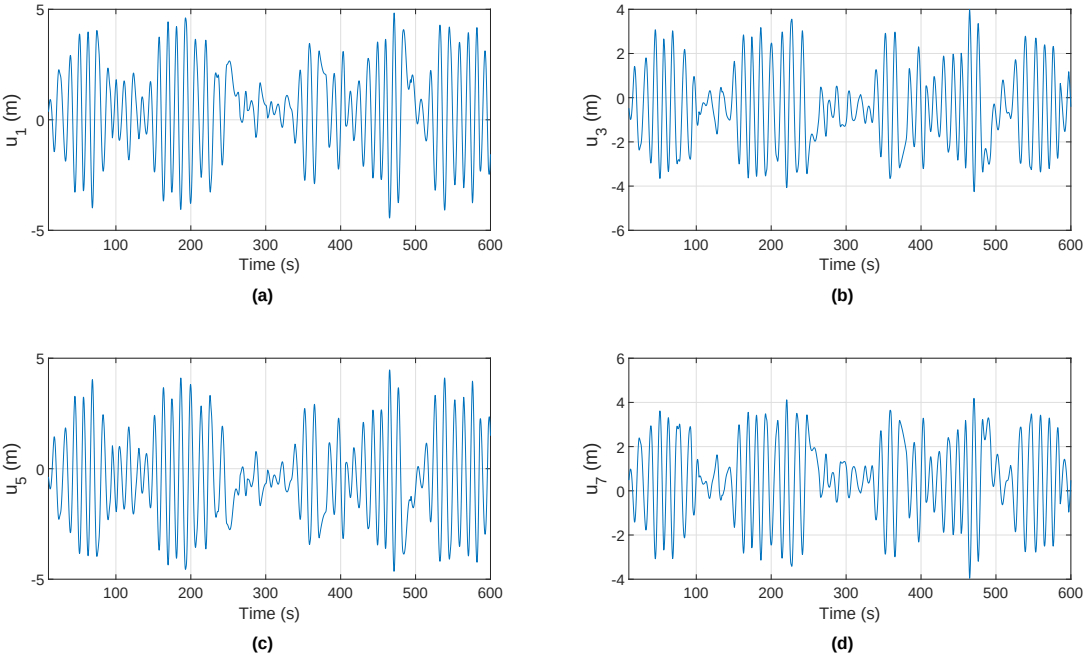

Figure 8. Liquid displacements u_1, u_3, u_5 and u_7 in the four vertical columns numbered 1, 3, 5 and 7 of the BTLCD reservoir for the transformed NREL 5-MW barge HWT model with the BTLCD configuration, in the extreme event for the tower-base fore-aft bending moment.

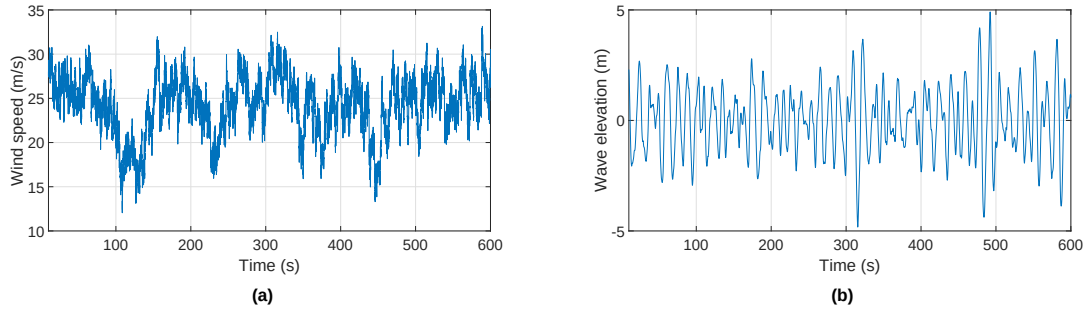

Figure 9. The hub-height longitudinal wind speed and wave elevation in the extreme event for the tower-base side-to-side bending moment.

6. CONCLUSIONS

We proposed to use the reservoir of the barge HWT as a BTLCD to damp the pitch and roll responses of the barge platform. To test performances of this spin-off application of the reservoir, we developed a detailed aero-hydro-servo-elastic barge HWT simulation model with a BTLCD reservoir: we first transformed the NREL 5-MW baseline barge wind turbine model within FAST into an HWT model and then modified the FAST code to incorporate the coupled dynamics of the barge-reservoir system into this HWT model by using Lagrange's equation. We applied multistart optimisation to derive the optimal parameters for the BTLCD reservoir based on two simplified mathematical models which describe the pitch and roll motions of the turbine-reservoir system, respectively. Through simulation studies under two types of extreme events and two types of normal events, we have shown that the BTLCD reservoir has effectively suppressed the barge pitch and roll motions, reducing the damage loads of the tower and the fluctuations of the rotor speed and generator power. Note that orifice damping plays an important role in TLCDs which has not be considered in the present study as only tuning effects have been considered.

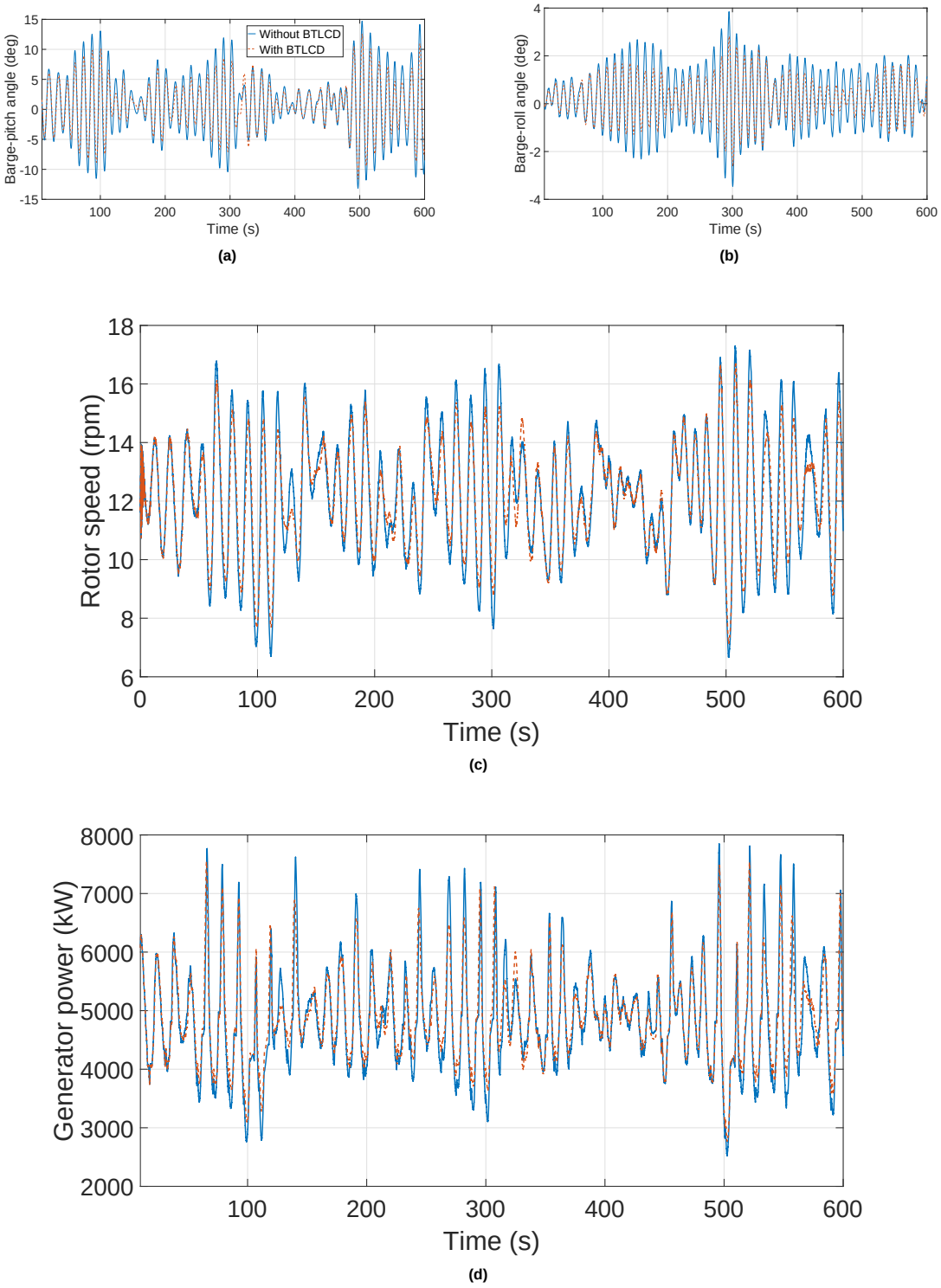

Figure 10. Simulations results for the transformed NREL 5-MW barge HWT model in the cases without (blue solid lines) and with (red dash lines) the BTLCD configuration, in the extreme event for the tower-base side-to-side bending moment. Figure 10a, 10b, 10c and 10d depict the barge pitch and roll displacements, the rotor speed and the generator power,respectively.

Wind Energ. 2018; **00**:1–?? © 2018 John Wiley & Sons, Ltd.
DOI: 10.1002/we
Prepared using weauth.cls

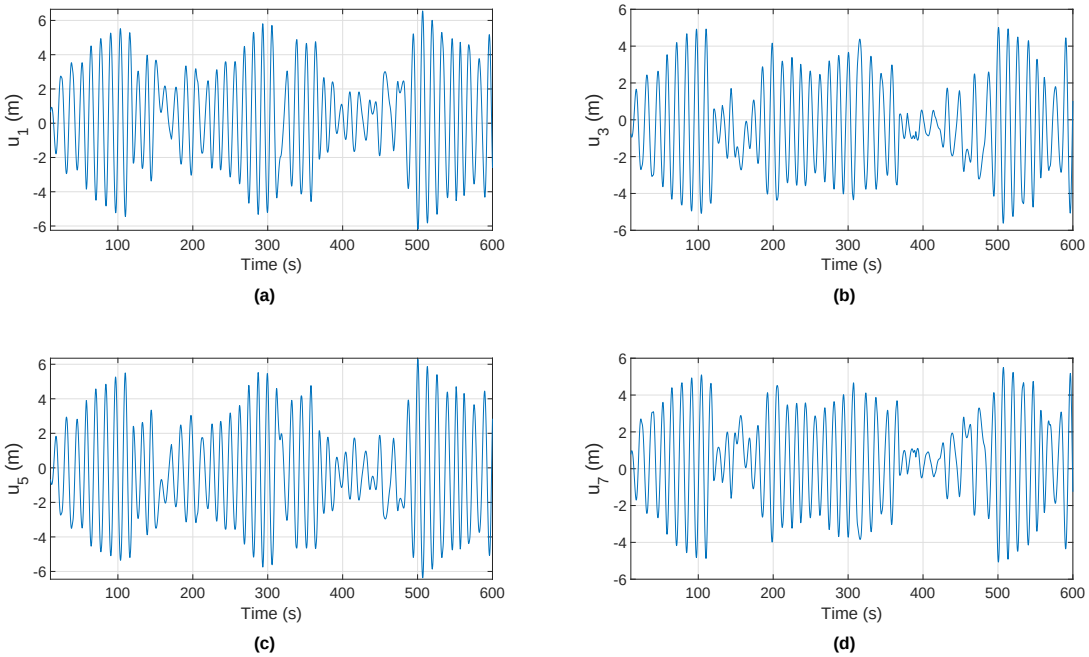

Figure 11. Liquid displacements u_1, u_3, u_5 and u_7 in the four vertical columns numbered 1, 3, 5 and 7 of the BTLCD reservoir for the transformed NREL 5-MW barge HWT model with the BTLCD configuration, in the extreme event for the tower-base side-to-side bending moment.

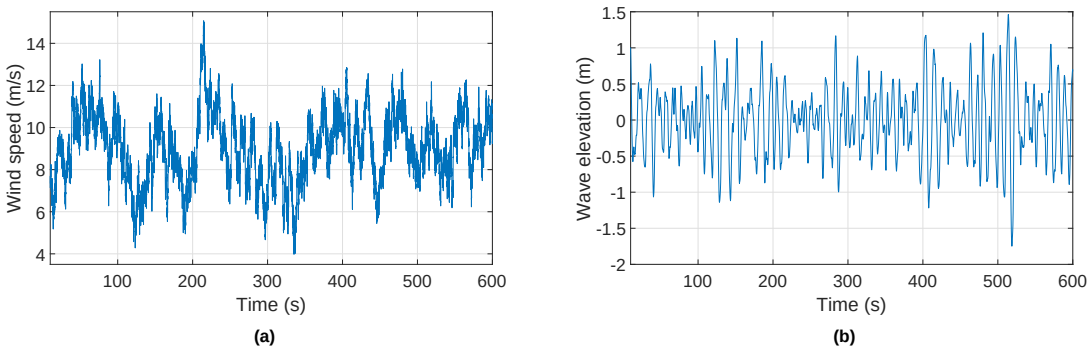

Figure 12. The hub-height longitudinal wind speed and wave elevation in the normal event where the mean hub-height longitudinal wind speed is 9 m/s.

REFERENCES

1. Ossyra JC, Patri S, Durbha V, Jankowski A. Reliable, lightweight transmissions for off-shore, utility scale wind turbines. *Technical Report*, Eaton Corporation, Innovation Center, 4201 N 27th Street, Milwaukee, WI 53216 2012.
2. Spinato F, Tavner P, Van Bussel G, Koutoulakos E. Reliability of wind turbine subassemblies. *IET Renewable Power Generation* 2009; **3**(4):387–401.
3. Ragheb A, Ragheb M. Wind turbine gearbox technologies. *Nuclear & Renewable Energy Conference (INREC), 2010 1st International*, Amman, Jordan, 2010; 1–8.
4. Staino A, Basu B. Dynamics and control of vibrations in wind turbines with variable rotor speed. *Engineering Structures* 2013; **56**:58–67.
5. Basu B, Staino A, Basu M. Role of flexible alternating current transmission systems devices in mitigating grid fault-induced vibration of wind turbines. *Wind energy* 2014; **17**(7):1017–1033.

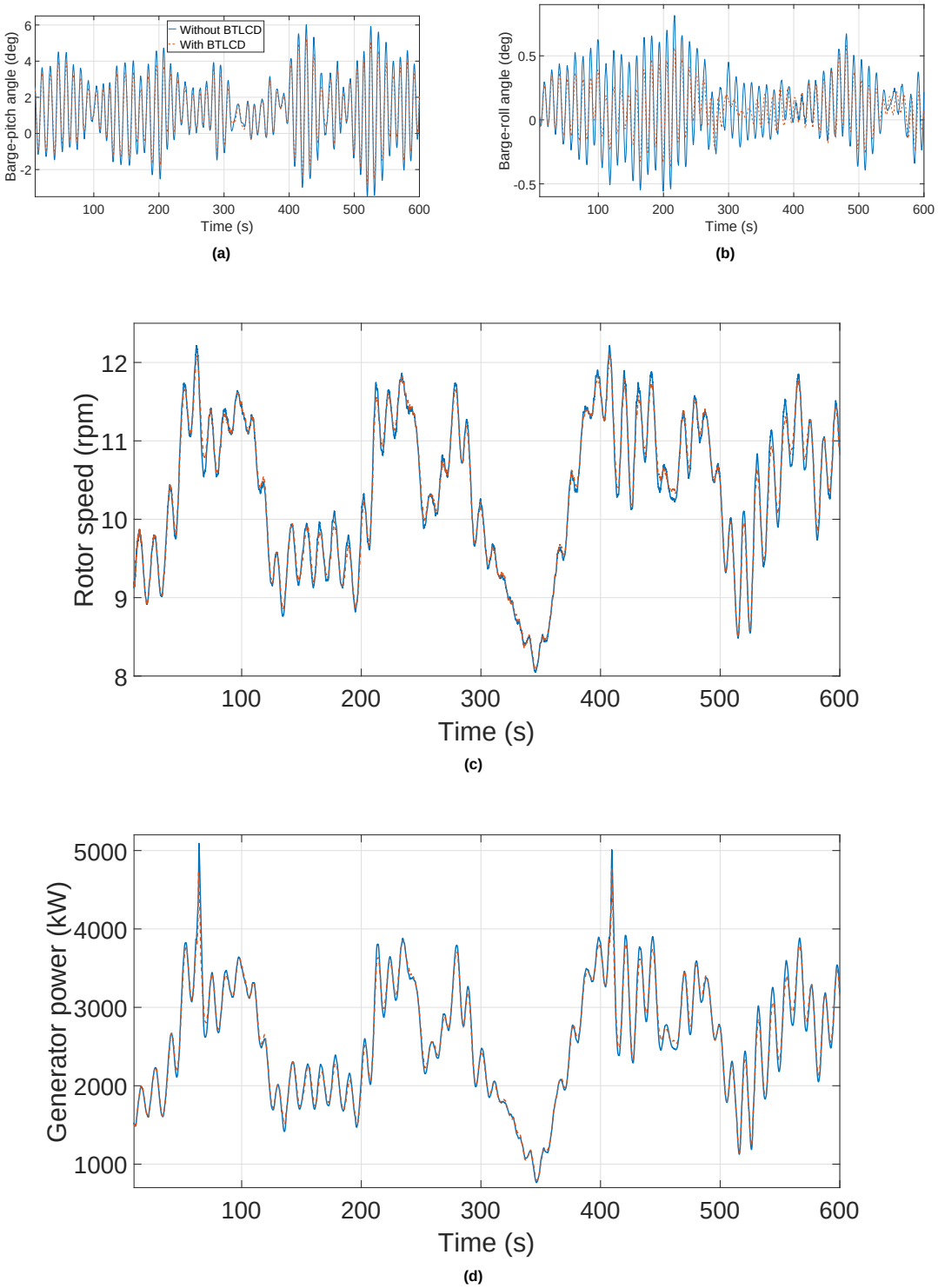

Figure 13. Simulations results for the transformed NREL 5-MW barge HWT model in the normal event where the mean hub-height longitudinal wind speed is 9 m/s. Figures 13a, 13b, 13c and 13d depict the barge pitch and roll displacements, the rotor speed, and the generator power, respectively.

Wind Energ. 2018; **00**:1–?? © 2018 John Wiley & Sons, Ltd.
DOI: 10.1002/we
Prepared using weauth.cls

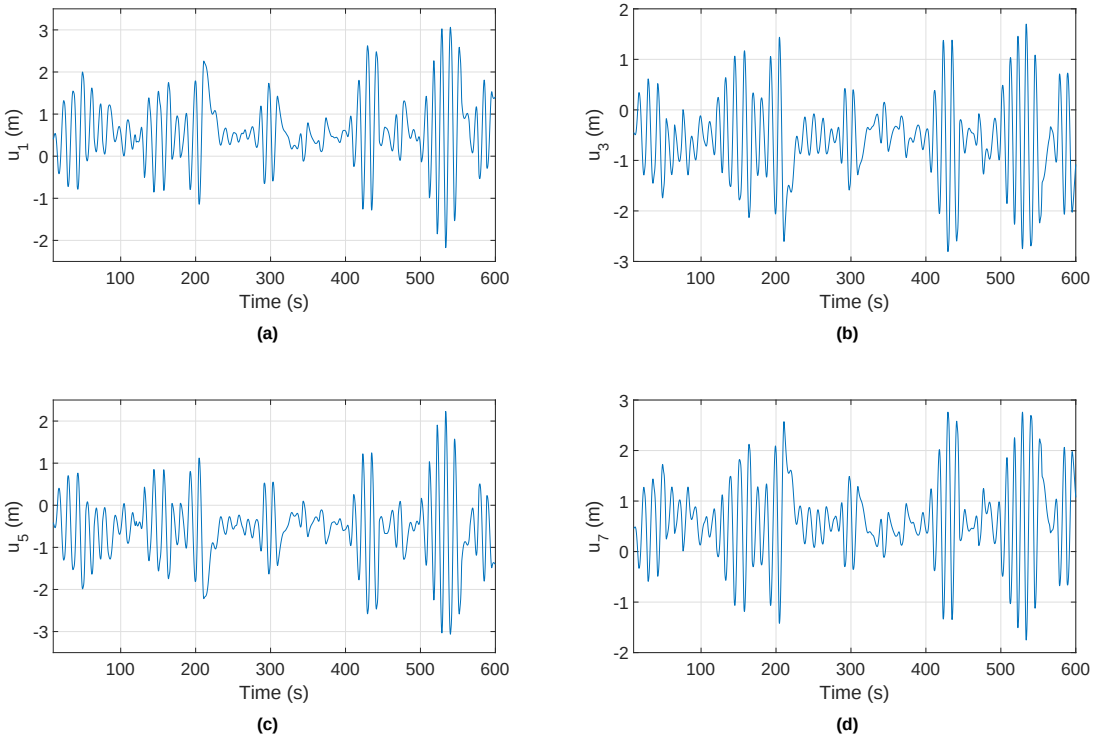

Figure 14. Liquid displacements u_1, u_3, u_5 and u_7 in the four vertical columns numbered 1, 3, 5 and 7 of the BTLCD reservoir for the transformed NREL 5-MW barge HWT model with the BTLCD configuration, in the normal event where the mean hub-height longitudinal wind speed is 9 m/s.

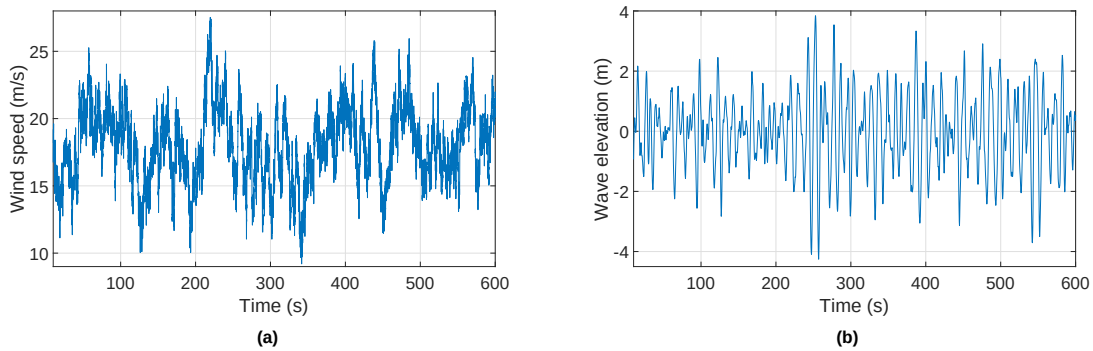

Figure 15. The hub-height longitudinal wind speed and wave elevation in the normal event where the mean hub-height longitudinal wind speed is 18 m/s.

6. Dutta R. Modeling and analysis of short term energy storage for mid-size hydrostatic wind turbine. Master's Thesis, University of Minnesota 2012.
7. Rapp J, Turesson J. Hydrostatic transmission in wind turbines: Development of test platform. Master's Thesis, Department of Management and Engineering, Division of Fluid and Mechatronic Systems, Linköping University 2015.
8. Zhao X, Weiss G. Suppression of the vibrations of wind turbine towers. *IMA Journal of Mathematical Control and Information* 2011; **28**:377–389.
9. Zhao X, Weiss G. Well-posedness and controllability of a wind turbine tower model. *IMA Journal of Mathematical Control and Information* 2011; **28**:103–119.

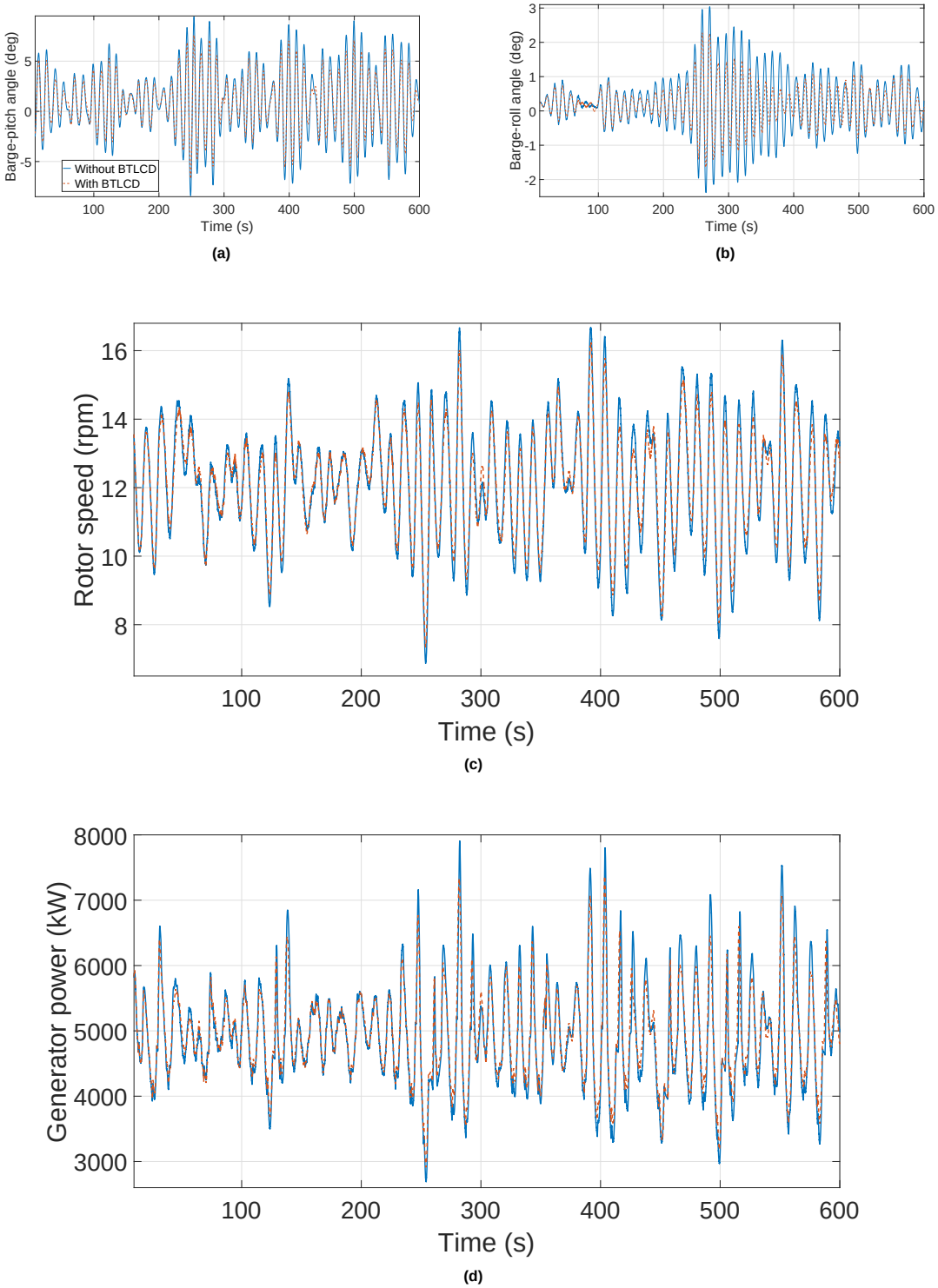

Figure 16. Simulations results for the transformed NREL 5-MW barge HWT model in the normal event where the mean hub-height longitudinal wind speed is 18 m/s. Figures 16a, 16b, 16c and 16d depict the barge pitch and roll displacements, the rotor speed, and the generator power, respectively.

Wind Energ. 2018; **00**:1–?? © 2018 John Wiley & Sons, Ltd.
DOI: 10.1002/we
Prepared using weauth.cls

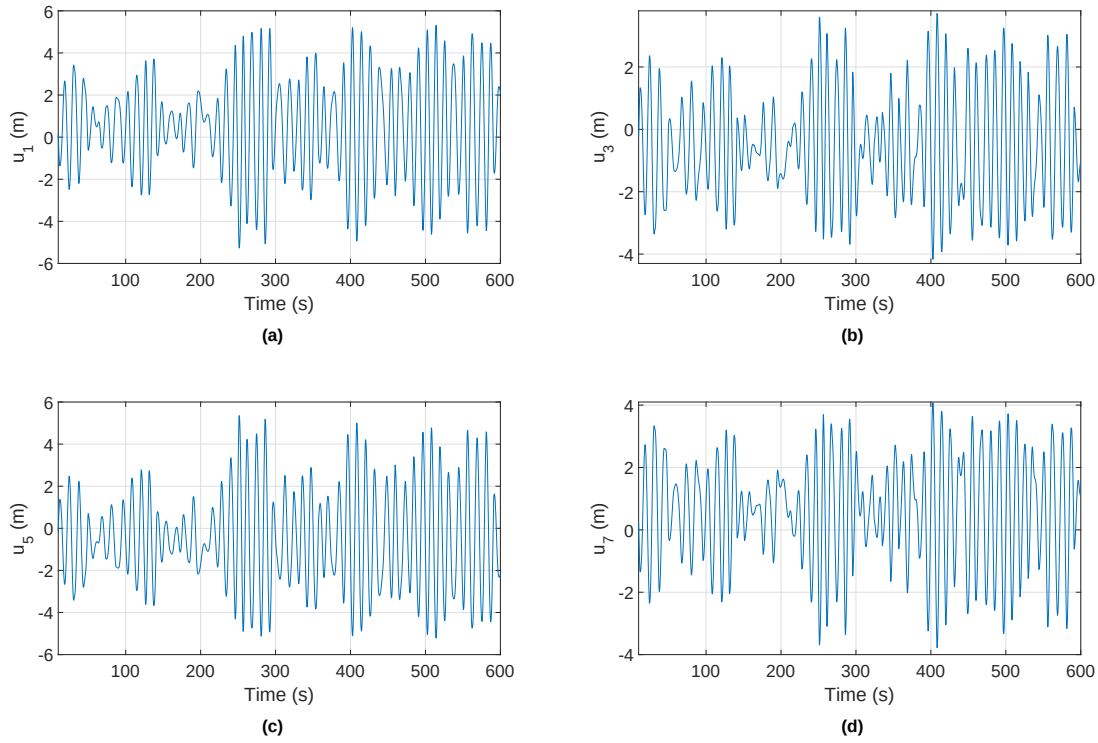

Figure 17. Liquid displacements u_1, u_3, u_5 and u_7 in the four vertical columns numbered 1, 3, 5 and 7 of the BTLCD reservoir for the transformed NREL 5-MW barge HWT model with the BTLCD configuration, in the normal event where the mean hub-height longitudinal wind speed is 18 m/s.

10. Dinh VN, Basu B, Nagarajaiah S. Semi-active control of vibrations of spar type floating offshore wind turbines. *Smart Structures and Systems* 2016; **18**(4):683–705.
11. Dinh VN, Basu B. Passive control of floating offshore wind turbine nacelle and spar vibrations by multiple tuned mass dampers. *Structural Control and Health Monitoring* 2015; **22**(1):152–176.
12. Staino A, Basu B, Nielsen SR. Actuator control of edgewise vibrations in wind turbine blades. *Journal of Sound and Vibration* 2012; **331**(6):1233–1256.
13. Fitzgerald B, Basu B, Nielsen SR. Active tuned mass dampers for control of in-plane vibrations of wind turbine blades. *Structural Control and Health Monitoring* 2013; **20**(12):1377–1396.
14. Jonkman JM. Dynamics modeling and loads analysis of an offshore floating wind turbine. *Technical Report*, National Renewable Energy Laboratory (NREL), Golden, Colorado, USA 2007.
15. Colwell S, Basu B. Experimental and theoretical investigations of equivalent viscous damping of structures with TLCD for different fluids. *Journal of structural engineering* 2008; **134**(1):154–163.
16. Bhattacharyya S, Ghosh A, Basu B. Experimental investigations into CLCD with identification of tuning and damping effects. *Journal of Structural Engineering* 2017; **143**(9):06017 003.
17. Balendra T, Wang C, Cheong H. Effectiveness of tuned liquid column dampers for vibration control of towers. *Engineering Structures* 1995; **17**(9):668–675.
18. Sadek F, Mohraz B, Lew H. Single-and multiple-tuned liquid column dampers for seismic applications. *Earthquake Engineering and Structural Dynamics* 1998; **27**(5):439–464.
19. Wu JC, Chang CH, Lin YY. Optimal designs for non-uniform tuned liquid column dampers in horizontal motion. *Journal of Sound and Vibration* 2009; **326**(1):104–122.
20. Chatterjee T, Chakraborty S. Vibration mitigation of structures subjected to random wave forces by liquid column dampers. *Ocean Engineering* 2014; **87**:151–161.
21. Chang C, Hsu C, Swei S. Control of buildings using single and multiple tuned liquid column dampers. *Structural Engineering and Mechanics* 1998; **6**(1):77–93.
22. Yalla SK, Kareem A. Optimum absorber parameters for tuned liquid column dampers. *Journal of Structural Engineering* 2000; **126**(8):906–915.

23. Gao H, Kwok K, Samali B. Optimization of tuned liquid column dampers. *Engineering structures* 1997; **19**(6):476–486.
24. Xue S, Ko J, Xu Y. Tuned liquid column damper for suppressing pitching motion of structures. *Engineering Structures* 2000; **22**(11):1538–1551.
25. Wu JC, Wang YP, Lee CL, Liao PH, Chen YH. Wind-induced interaction of a non-uniform tuned liquid column damper and a structure in pitching motion. *Engineering Structures* 2008; **30**(12):3555–3565.
26. Colwell S, Basu B. Tuned liquid column dampers in offshore wind turbines for structural control. *Engineering Structures* 2009; **31**(2):358–368.
27. Roderick C. Vibration reduction of offshore wind turbines using tuned liquid column dampers. Master's Thesis, University of Massachusetts Amherst 2012.
28. Coudurier C, Lepreux O, Petit N. Passive and semi-active control of an offshore floating wind turbine using a tuned liquid column damper. *IFAC-PapersOnLine* 2015; **48**(16):241–247.
29. Basu B, Zhang Z, Nielsen SR. Damping of edgewise vibration in wind turbine blades by means of circular liquid dampers. *Wind Energy* 2016; **19**(2):213–226.
30. Hitchcock P, Kwok K, Watkins R, Samali B. Characteristics of liquid column vibration absorbers (LCVA)—II. *Engineering Structures* 1997; **19**(2):135–144.
31. Lee SK, Min KW, Lee HR. Parameter identification of new bidirectional tuned liquid column and sloshing dampers. *Journal of Sound and Vibration* 2011; **330**(7):1312–1327.
32. Rozas L, Boroschek RL, Tamburrino A, Rojas M. A bidirectional tuned liquid column damper for reducing the seismic response of buildings. *Structural Control and Health Monitoring* 2016; **23**(4):621–640.
33. Jonkman B, Jonkman J. *FAST v8.16.00a-bjj*. National Renewable Energy Laboratory, CO, USA 2016.
34. Jonkman BJ. TurbSim user's guide: Version 1.50. *Technical Report*, National Renewable Energy Laboratory (NREL), Golden, Colorado, USA 2009.
35. International Electrotechnical Commission, Geneva, Switzerland. *Wind Turbines—Part 1: Design Requirements*. 3 edn. 2005.
36. Jonkman JM, Buhl Jr ML. FAST user's guide. *Technical Report*, National Renewable Energy Laboratory (NREL), Golden, Colorado, USA 2005.
37. Platt A, Jonkman B, Jonkman J. InflowWind user's guide. *Technical Report*, National Wind Technology Center, CO, USA 2016.
38. Jonkman J, Robertson A, Hayman G. HydroDyn user's guide and theory manual. *Technical Report*, National Renewable Energy Laboratory, CO, USA 2014.
39. Tong X, Zhao X. LPV pitch control of a hydrostatic wind turbine based on LIDAR preview. *2017 American Control Conference*, WA, USA, 2017.
40. Tong X, Zhao X. Power generation control of a monopile hydrostatic wind turbine using an $\mathcal{H}_\infty$ loop-shaping torque controller and an LPV pitch controller. *IEEE Transactions on control systems technology* 2017; DOI: 10.1109/TCST.2017.2749562.
41. Tong X, Zhao X, Zhao S. Load reduction of a monopile wind turbine tower using optimal tuned mass dampers. *International Journal of Control* 2017; **90**(7):1283–1298.
42. Ghosh A, Basu B. A closed-form optimal tuning criterion for TMD in damped structures. *Structural Control and Health Monitoring* 2007; **14**(4):681–692.
43. Hayman G. MLife theory manual for version 1.00. *Technical Report*, National Renewable Energy Laboratory (NREL), Golden, Colorado, USA 2012.
44. Stewart G, Lackner MA. Offshore wind turbine load reduction employing optimal passive tuned mass damping systems. *IEEE Transactions on Control Systems Technology* 2013; **21**(4):1090–1104.

DOI: 10.1002/we
Prepared using weauth.cls

Table I. Tower-base fore-aft and side-to-side DEQLs of the transformed NREL 5-MW barge HWT model in the cases without and with the BTLCD configuration under two extreme events for the tower-base fore-aft bending moment (Event E.1) and the side-to-side bending moment (Event E.2), as well as the load reduction ratios (in the brackets) by the BTLCD.

	Event E.1		Event E.2	
	Fore-aft DEQL (kN)	Side-to-side DEQL (kN)	Fore-aft DEQL (kN)	Side-to-side DEQL (kN)
Without BTLCD	83435	25131	121910	32045
With BTLCD	73324 (12.11%)	18195 (27.6%)	104300 (14.45%)	25756 (19.63%)

Table II. Tower-base fore-aft and side-to-side DEQLs of the transformed NREL 5-MW barge HWT model in the cases without and with the BTLCD configuration under two normal events where the mean hub-height longitudinal wind speeds are 9 m/s (Event N.1) and 18 m/s (Event N.2) respectively, as well as the load reduction ratios (in the brackets) by the BTLCD.

	Event N.1		Event N.2	
	Fore-aft DEQL (kN)	Side-to-side DEQL (kN)	Fore-aft DEQL (kN)	Side-to-side DEQL (kN)
Without BTLCD	48968	9385.3	105920	26423
With BTLCD	43894 (10.36%)	7121.9 (24.12%)	91703 (13.42%)	20122 (23.85%)